Hu et al. Nanoscale Research Letters (2016) 11:257
DOI 10.1186/s11671-016-1475-9

Nanoscale Research Letters

NANO EXPRESS Open Access

Hierarchical Heterostructures of $NiCo_2O_4$@$XMoO_4$ (X = Ni, Co) as an Electrode Material for High-Performance Supercapacitors

Jiyu Hu[1], Feng Qian[1*], Guosheng Song[2] and Linlin Wang[3*]

Abstract

Hierarchical heterostructures of $NiCo_2O_4$@$XMoO_4$ (X = Ni, Co) were developed as an electrode material for supercapacitor with improved pseudocapacitive performance. Within these hierarchical heterostructures, the mesoporous $NiCo_2O_4$ nanosheet arrays directly grown on the Ni foam can not only act as an excellent pseudocapacitive material but also serve as a hierarchical scaffold for growing $NiMoO_4$ or $CoMoO_4$ electroactive materials (nanosheets). The electrode made of $NiCo_2O_4$@$NiMoO_4$ presented a highest areal capacitance of 3.74 F/cm^2 at 2 mA/cm^2, which was much higher than the electrodes made of $NiCo_2O_4$@$CoMoO_4$ (2.452 F/cm^2) and $NiCo_2O_4$ (0.456 F/cm^2), respectively. Meanwhile, the $NiCo_2O_4$@$NiMoO_4$ electrode exhibited good rate capability. It suggested the potential of the hierarchical heterostructures of $NiCo_2O_4$@$CoMoO_4$ as an electrode material in supercapacitors.

Keywords: Supercapacitor, $NiCo_2O_4$@$XMoO_4$, Heterostructures, Nanosheet arrays

Background

To meet the increasing requirement for portable electronics, hybrid electronic vehicles and other micro- and nanodevices, numerous studies have been carried out to develop many kinds of energy storage systems. As an important energy storage device, the widely studied supercapacitors, also known as electrochemical capacitors, have been believed as a promising candidate due to their high specific power, long cycling life, fast charge and discharge rates, and reliable safety [1–9]. Though these supercapacitors demonstrated these distinctive advantages, as compared with the batteries and fuel cells, the relatively lower energy densities seriously block their large-scale practical application [4, 10]. So far, various electrode materials which include carbon materials [11, 12], transition metal oxides [2, 13–15], and conducting polymers [16, 17] have been designed and synthesized to enhance the electrochemical properties for the practical applications in the supercapacitors.

Recently, some bimetallic oxides, such as $NiCo_2O_4$ [15, 17–20], $ZnCo_2O_4$ [21, 22], $NiMoO_4$ [23], and $CoMoO_4$ [24, 25], have been developed as a new electrode material used for supercapacitors because of their excellent electrical conductivity and multiple oxidation states (as compared with the binary metal oxides) for reversible Faradaic reactions [26]. For fully utilizing the advantages of active materials and thus optimizing the performance of these materials, plenty of efforts has been devoted, i.e., realizing additive/binder-free electrode architectures, which eliminate the "dead surface" and release complicated process in traditional slurry-coating electrode and meaningfully improve the utilization rate of electrode materials even at high rates [4, 27], constructing 3D hierarchical heterostructures, which can provide efficient and fast pathways for electron and ion transport [20, 28], and exploring smart integrated array architectures with rational multi-component combination, which can achieve the synergistic effect from all individual constituents [29–31]. Taken some successful examples, Co_xNi_{1-x}DHs/$NiCo_2O_4$/CFP composite electrodes were

* Correspondence: apfenqian@126.com; wlinlin@sues.edu.cn
[1]No. 2 High School of East China Normal University, Shanghai 201203, China
[3]College of Chemistry and Chemical Engineering, Shanghai University of Engineering Science, Shanghai 201620, China
Full list of author information is available at the end of the article

prepared by a hydrothermal route and an electrodeposition process, showing high capacitance of ~1.64 F/cm^2 at 2 mA/cm^2, good rate capability, and excellent cycling stability [20]; 3D hierarchical $NiCo_2O_4$@$NiMoO_4$ core-shell nanowire/nanosheet arrays delivered a high areal capacitance of 5.80 F/cm^2 at 10 mA/cm^2, excellent rate capability, and high cycling stability [32]. Despite these notable achievements, it is still a hard task to design and construct 3D hierarchical heterostructures made of the bimetallic oxides with improved electrochemical properties for the supercapacitors.

Herein, we report hydrothermal growth of hierarchical heterostructures of $NiCo_2O_4$@$XMoO_4$ (X = Ni, Co) as an electrode material for the supercapacitors with improved performances. Within these hierarchical heterostructures, high electrochemical activity of $NiCo_2O_4$ not only shows outstanding pseudocapacity but also can be regarded as a backbone to provide reliable electrical connection to the $XMoO_4$ (X = Ni, Co). Between them, the $NiCo_2O_4$@$NiMoO_4$ electrode material showed a highest areal capacitance of 3.74 F/cm^2 at 2 mA/cm^2, which was much higher than the $NiCo_2O_4$@$CoMoO_4$ electrode material (2.452 F/cm^2), and good rate capability, implying its prospect as an alternative electrode material in the supercapacitors.

Methods

Synthesis of $NiCo_2O_4$@$XMoO_4$ (X = Ni, Co) Composite Nanosheet Arrays

All the reactants here were analytically graded and used without further purification. The synthesis of the composite nanosheet arrays was described briefly as follows: Firstly, the $NiCo_2O_4$ nanosheet arrays were grown on the Ni foam according to a reference [17]. Secondly, the product of as-grown $NiCo_2O_4$ nanosheet arrays was put into a 60-mL Teflon-lined autoclave, which contained 0.5 mmol of $NiCl_2{\cdot}6H_2O$ (or $CoCl_2{\cdot}6H_2O$), 0.5 mmol of $Na_2MoO_4{\cdot}2H_2O$, and 50 mL of deionized water. The autoclave was sealed and maintained at 120 °C for 2 h (or 1 h) in an electric oven and then cooled down to room temperature. The $NiCo_2O_4$@$XMoO_4$ (X = Ni, Co) composites on the Ni foam were carefully washed with deionized water and absolute ethanol, successively, and then dried at 60 °C overnight. Lastly, the samples were annealed at 400 °C for 1 h at a ramping rate of 1 °C/min.

Material Characterizations

As-synthesized products were characterized by means of a D/max-2550 PC X-ray diffractometer (XRD; Rigaku, Cu-Kα radiation), a scanning electron microscopy (SEM; S-4800), and a transmission electron microscopy (TEM; JEM-2100 F) equipped with an energy-dispersive X-ray spectrometer (EDX).

Results and Discussion

In this work, the $NiCo_2O_4$@$XMoO_4$ (X = Ni, Co) hierarchical heterostructures were successfully synthesized for electrode materials. As depicted schematically in Fig. 1, the synthesis process includes two steps: the hydrothermal growth of $NiCo_2O_4$ nanosheets on the Ni foam and subsequent annealing as the first step and the hydrothermal growth of $NiMoO_4$ or $CoMoO_4$ nanosheets (coatings) on the $NiCo_2O_4$ nanosheet arrays and another annealing process as the second step. Herein, 3D Ni foam, with uniform macropore structure, huge supporting area, and high electrical conductivity, was selected as a current collector for the growth of electrode materials, which can provide efficient electrolyte penetration to enable fast ion diffusion [27, 33]. Meanwhile, the $NiCo_2O_4$ nanosheets grown uniformly on Ni foam functioned as the backbone to support and give reliable electrical connection to $XMoO_4$ (X = Ni, Co) nanosheets, which can contribute to electronic and ionic diffusion and improve the utilization rate of electrode material. More importantly, the $NiCo_2O_4$ electrode material with high electrochemical activity can also act as active materials for charge storage and contribute to the capacitance.

Combining the hydrothermal reaction and the annealing process resulted in the $NiCo_2O_4$ nanosheet arrays grown on Ni foam. Detailed morphology and microstructure of the $NiCo_2O_4$ nanosheets were investigated via the scanning electron microscopy (SEM) and transmission electron microscopy (TEM). Figure 2a, b shows the highly tight $NiCo_2O_4$ nanosheets (with a thickness of

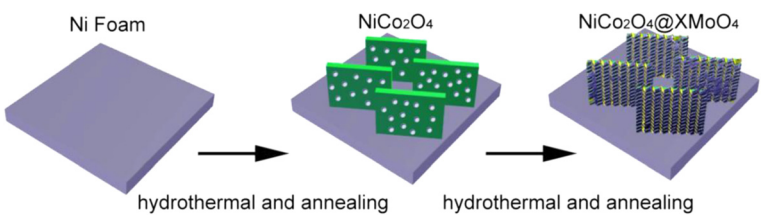

Fig. 1 Schematic depicting the growth process of the hierarchical heterostructures of the $NiCo_2O_4$@$XMoO_4$ (X = Ni, Co)

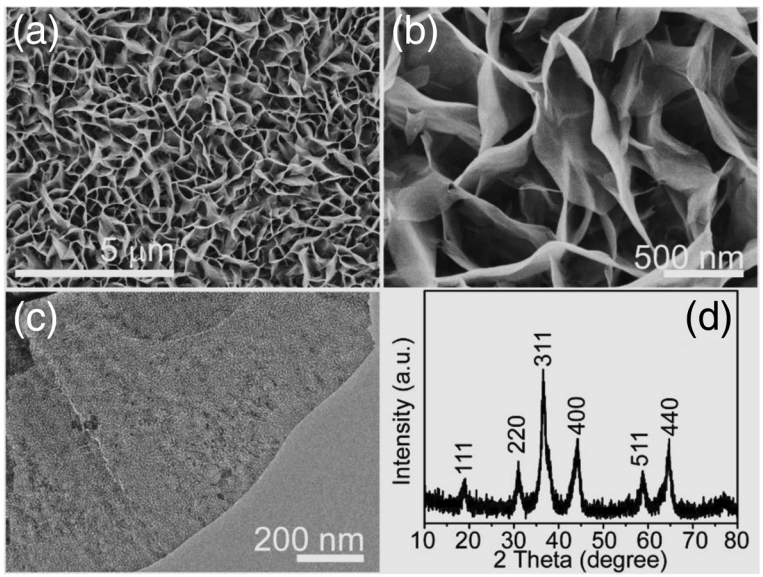

Fig. 2 **a**, **b** Low- and high-magnification SEM images of as-prepared $NiCo_2O_4$ nanosheet arrays on the Ni foam. **c** TEM image of a $NiCo_2O_4$ nanosheet. **d** XRD pattern of the product scratched from the Ni foam

~30–50 nm) that grew uniformly and vertically on the Ni foam and interconnected with each other, resulting in a highly porous structure with an abundant open space. Figure 2c shows a $NiCo_2O_4$ nanosheet almost transparent to electron beam, suggesting an ultrathin feature. Intriguingly, numerous mesoporous arrays are distributed uniformly throughout the whole $NiCo_2O_4$ nanosheet. The nanosheet arrays were scratched from the Ni foam and were then characterized by X-ray diffraction (XRD) to determine the crystalline phase of the product. As shown in Fig. 2d, all well-defined diffraction peaks can be indexed to the cubic phase $NiCo_2O_4$ by referring to the JCPDS card (no. 20-0781).

The $NiCo_2O_4$ nanosheet arrays grown on the Ni foam act as an ideal scaffold to load additional electroactive pseudocapacitive materials, thus enhancing the electrochemical performance. Considering this merit, $NiMoO_4$ or $CoMoO_4$ nanosheets were grown on the surface of the $NiCo_2O_4$ nanosheets via a hydrothermal reaction and an annealing step similar to the first growth step described above, forming $NiCo_2O_4$@$NiMoO_4$ composite nanosheet arrays (a core-shell structure or shaped like caterpillar). Figure 3a, b shows SEM images of the $NiCo_2O_4$@$NiMoO_4$ composite nanosheet arrays, in which the ultrathin $NiMoO_4$ nanosheets were uniformly grown on the surface of $NiCo_2O_4$ nanosheets and thus plenty of the space among $NiCo_2O_4$ nanosheets is utilized abundantly, and a thickness of the $NiCo_2O_4$@-$NiMoO_4$ composite nanosheets is in the range of ~250–300 nm. Importantly, the integration of the $NiMoO_4$ material into the original $NiCo_2O_4$ nanosheet arrays does not destroy the ordered structure. In addition, these $NiMoO_4$ nanosheets are interconnected with each other to form a highly porous morphology, which can provide more active sites for electrolyte ions to transport efficiently. Figure 3c shows the TEM image of the $NiCo_2O_4$@$NiMoO_4$ composites. The result shows that the $NiMoO_4$ nanosheets are highly dense but still do not cover the entire mesoporous $NiCo_2O_4$ nanosheets fully. Moreover, energy-dispersive X-ray (EDX) spectrum (Fig. 3d) indicates that Ni, Co, Mo, and O can be detected in the composites. Surely, the Cu and C signals come from the carbon-supported Cu grid.

Figure 4 shows the SEM images of the samples, prepared via a different hydrothermal reaction time. It is used to demonstrate the formation process of the samples. Figure 4a depicts the $NiCo_2O_4$@$NiMoO_4$ nanosheet arrays formed via 0.5 h of the hydrothermal reaction. It can be seen that the nanosheets' surface of $NiCo_2O_4$ loses their original smooth appearance and was interspersed by many fine $NiMoO_4$ nanosheets. Then, the reaction time was extended to 1 h and the SEM image (Fig. 4b) showed the results. Almost all the naked surface observed before was fully coated by $NiMoO_4$ nanosheets with the thickness increased to ~100–150 nm. As the time of the hydrothermal reaction becomes longer, the composition becomes thicker and at last the whole thickness in Fig. 4d is ~400–500 nm, which leads to a much smaller interspace among the adjacent sheets. But the growth of mass $NiMoO_4$ nanosheets on the $NiCo_2O_4$ nanosheets may decay the utilization of the $NiCo_2O_4$ (core) materials and even some $NiMoO_4$ (shell) materials

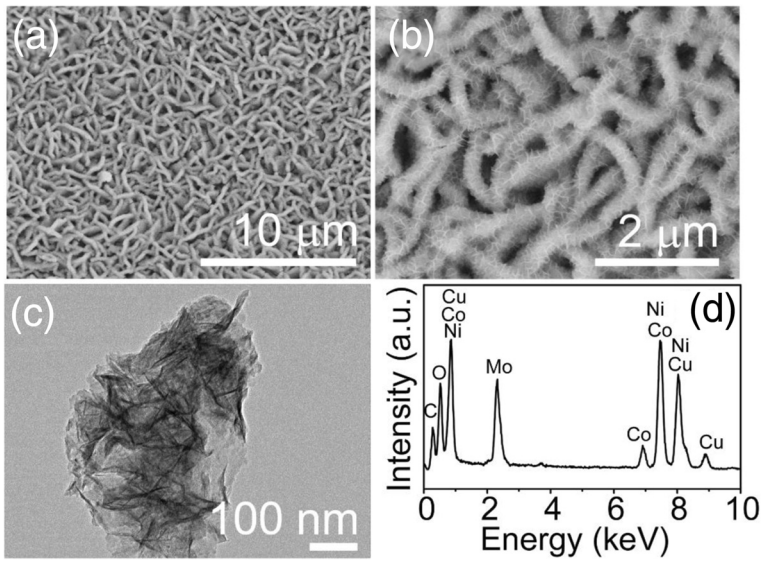

Fig. 3 **a**, **b** Low- and high-magnification SEM images of the hierarchical heterostructures of the $NiCo_2O_4$@$NiMoO_4$ composite nanosheet arrays on the Ni foam. **c** TEM image and (**d**) EDX spectrum of the $NiCo_2O_4$@$NiMoO_4$ composite nanosheet arrays

may be blocked from the access to electrolyte. Therefore, the hydrothermal reaction time should be optimized (e.g., 2 h) to get an improved electrochemical properties.

Hierarchical heterostructures of the $NiCo_2O_4$@$CoMoO_4$ composite nanosheets were also fabricated as a comparison with the $NiCo_2O_4$@$NiMoO_4$ nanosheet arrays for their usage as an electrode material. Figure 5a, b shows the SEM image of the $NiCo_2O_4$@$CoMoO_4$ composite nanosheets. It clearly confirms that the whole surface of the $NiCo_2O_4$ nanosheets is homogeneously covered by the $CoMoO_4$ nanosheets, and the uniformity of these structures is similar to that of the $NiCo_2O_4$@$NiMoO_4$ nanosheet arrays. As the TEM image (Fig. 5c) demonstrates, the thickness of the $CoMoO_4$ nanosheets is about 20–50 nm. Additionally, the composition of the as-synthesized $NiCo_2O_4$@$CoMoO_4$ composites was confirmed by EDX. As shown in Fig. 5d, the peaks of Cu and C derive from the Cu grid, and the strong signals of Ni, Co, Mo, and O further ascertain the formation of $NiCo_2O_4$@$CoMoO_4$.

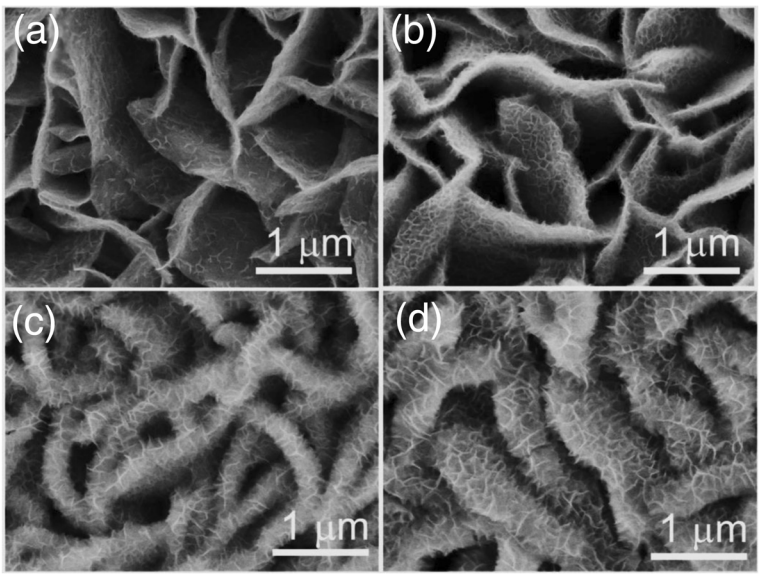

Fig. 4 SEM images of the morphology evolution of the $NiCo_2O_4$@$NiMoO_4$ nanosheet arrays formed via different reaction time: (**a**) 0.5 h, (**b**) 1 h, (**c**) 2 h, and (**d**) 4 h

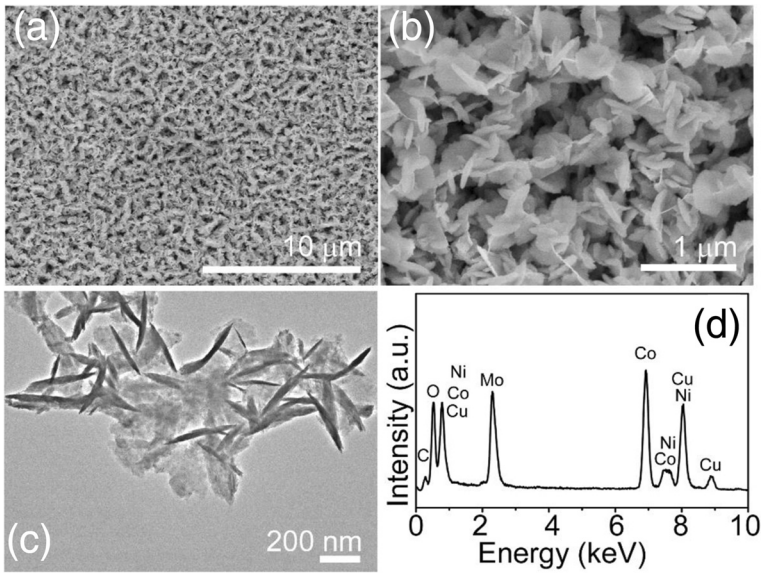

Fig. 5 **a**, **b** Low- and high-magnification SEM images and **c** TEM image of the hierarchical heterostructures of the $NiCo_2O_4$@$CoMoO_4$ composite nanosheets. **d** EDX spectrum of the $NiCo_2O_4$@$CoMoO_4$ composite nanosheet arrays

Then, the electrochemical properties of the hierarchical heterostructures of the $NiCo_2O_4$@$XMoO_4$ (X = Ni, Co) were investigated to evaluate their applicability as an active material for the supercapacitors, where a three-electrode cell with a saturated calomel electrode (SCE) reference electrode, a Pt counter electrode, and a KOH aqueous electrolyte (3 M) inside was used. As a comparison, the cyclic voltammogram (CV) curves from three electrodes made from $NiCo_2O_4$ and $NiCo_2O_4$@$XMoO_4$ (X = Ni, Co) materials, respectively, were shown in Fig. 6a. It was recorded with a potential window ranging from 0 to 0.6 V and a scan rate of 5 mV/s. Deduced from the CV curves' shape, the Faradaic redox reactions associated with M-O/M-O-OH (M = Ni, Co) dominated the capacitance characteristics [18, 20] of these electrodes. Obviously, the surface area of the $NiCo_2O_4$@$NiMoO_4$ electrode is higher than that of the $NiCo_2O_4$@$CoMoO_4$ electrode and $NiCo_2O_4$ electrode, suggesting that the $NiCo_2O_4$@$NiMoO_4$ electrode

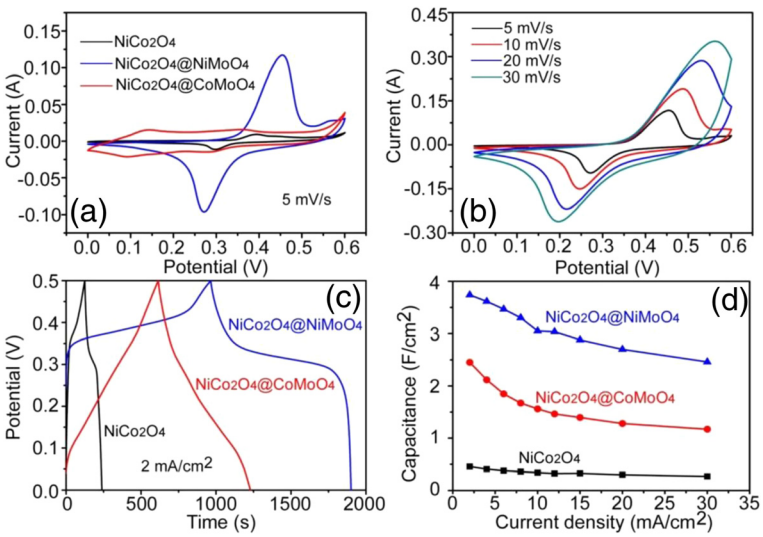

Fig. 6 **a** CV curves of the $NiCo_2O_4$@$XMoO_4$ (X = Ni, Co) and $NiCo_2O_4$ electrodes at a scan rate of 5 mV/s. **b** CV curves of the $NiCo_2O_4$@$NiMoO_4$ electrode at a various scan rate, i.e., 5, 10, 20, and 30 mV/s. **c** CD curves of the $NiCo_2O_4$@$XMoO_4$ (X = Ni, Co) and $NiCo_2O_4$ electrodes collected at a current density of 2 mA/cm^2. **d** Areal capacitance of the $NiCo_2O_4$@$XMoO_4$ (X = Ni, Co) and the $NiCo_2O_4$ electrodes calculated from the CD curves as a function of current density

possessed a greater capacitance than the other two. The high capacitance of the $NiCo_2O_4$@$NiMoO_4$ electrode is mainly attributed to the fact that a highly porous nanostructure that originated from numerous ultrathin $NiMoO_4$ nanosheets grown on the $NiCo_2O_4$ nanosheet surface should provide more active sites for increasing electrolyte ion transportation efficiency to enhance the utilization of the whole electrode. Also, the CV curves of the $NiCo_2O_4$@$NiMoO_4$ electrodes taken via a various scan rate, i.e., 5, 10, 20, and 30 mV/s, were collected, as shown in Fig. 6b. It was noted that the peak position shifted slightly with the increase of scan rate, implying a good capacitive behavior and a high-rate capability of the electrode material. The galvanostatic charge-discharge (CD) method was applied to compare the capacitive ability of the $NiCo_2O_4$ electrode and two composite electrodes of $NiCo_2O_4$@$NiMoO_4$ and $NiCo_2O_4$@$CoMoO_4$ at the same current density of 2 mA/cm^2, as illustrated in Fig. 6c. It was found that the $NiCo_2O_4$@$NiMoO_4$ electrode possessed a longer discharging time than the $NiCo_2O_4$@$CoMoO_4$ and pure $NiCo_2O_4$ electrodes, demonstrating that such an electrode has an enhanced capacitance. Moreover, the areal capacitance of the electrode materials could be calculated from their CD curves by this equation: $C = (I \cdot t)/(S \cdot \Delta V)$, where I (A) is the current for the charge-discharge measurement, t (s) is the discharge time, S is the geometrical area of the electrode [31], and ΔV (V) is the voltage interval of the discharge. As shown in Fig. 6d, the $NiCo_2O_4$@$NiMoO_4$ electrode always exhibited higher areal capacitances than the $NiCo_2O_4$@$CoMoO_4$ and $NiCo_2O_4$ electrodes. The maximal areal capacitance of the $NiCo_2O_4$@$NiMoO_4$ electrode was found to be 3.74 F/cm^2 at 2 mA/cm^2, which is much higher than the $NiCo_2O_4$@$CoMoO_4$ electrode (2.45 F/cm^2), and 8 times higher than the $NiCo_2O_4$ electrode (0.46 F/cm^2). In particular, the $NiCo_2O_4$@$NiMoO_4$ electrode still has an areal capacitance of 2.46 F/cm^2 even if the current density increased to 30 mA/cm^2, retaining appropriately 66 % of its initial value. However, the $NiCo_2O_4$@$CoMoO_4$ electrode and the $NiCo_2O_4$ electrode only showed the areal capacitance of 1.17 and 0.27 F/cm^2 at a high current density of 30 mA/cm^2, respectively.

Figure 7 shows the cycling performance of the $NiCo_2O_4$@$XMoO_4$ (X = Ni, Co) composite electrodes, which was evaluated through 2000 cycles with a scan rate of 60 mV/s. After 2000 cycles, it is found that the total capacitance retention was ~95.5 % for the $NiCo_2O_4$@$CoMoO_4$ electrode and ~83.1 % for the $NiCo_2O_4$@$NiMoO_4$ electrode, respectively. Compared with the $NiCo_2O_4$@$CoMoO_4$ electrodes, the $NiCo_2O_4$@$NiMoO_4$ electrode did not show a better cycling stability, but the characteristics of the high-rate capability and the large areal capacitance make the hierarchical heterostructures of the $NiCo_2O_4$@$NiMoO_4$ a more prospective electrode material. The outstanding capacitive properties of

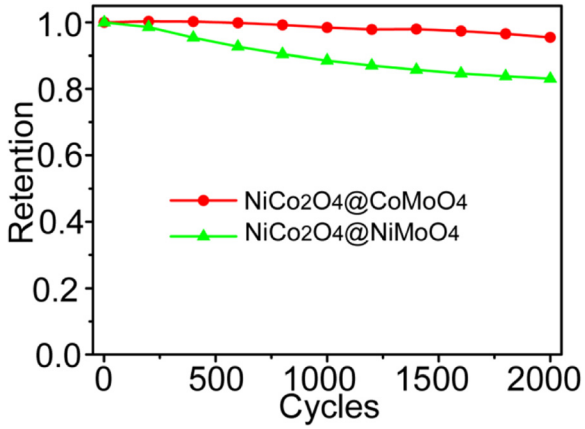

Fig. 7 Cycling performance of the $NiCo_2O_4$@$XMoO_4$ (X = Ni, Co) composite electrodes at a scan rate of 60 mV/s for 2000 cycles

the hierarchical heterostructures of the $NiCo_2O_4$@$XMoO_4$ (X = Ni, Co) electrode are considered to originate from the synergistic effect of its following distinctive compositional and topological features [34–36]. First, within the hierarchical heterostructures, both core and shell are active materials, and the core-shell heterostructures enable easy access of electrolyte. Therefore, both of them can effectively contribute to the capacity. Secondly, the $NiCo_2O_4$ is highly conductive, which can provide "superhighways" for the charge in the core-shell structure. The direct growth of the $XMoO_4$ nanosheets on the $NiCo_2O_4$ nanosheet arrays avoids the use of polymer binder/conductive additives and further guarantees the effective charge transport between them. Besides, the high electrical conductivity could decrease the charge transfer resistance of the electrodes, thus leading to an increased power density. Finally, the $XMoO_4$ nanosheets and the $NiCo_2O_4$ nanosheets are mesoporous that increases the electroactive sites.

Conclusions

In conclusion, 3D hierarchical heterostructures of the $NiCo_2O_4$@$XMoO_4$ (X = Ni, Co) composite nanosheet arrays have been successfully designed and prepared for the supercapacitors. In such a novel nanostructure, the mesoporous $NiCo_2O_4$ nanosheet arrays grown directly on the Ni foam not only acted as a good pseudocapacitive material but also used as a hierarchical framework for loading $NiMoO_4$ or $CoMoO_4$ electroactive material. Notably, the $NiCo_2O_4$@$NiMoO_4$ composite electrode showed excellent rate capability as well as a highest areal capacitance of 3.74 F/cm^2 at 2 mA/cm^2, which was much higher than the values for the $NiCo_2O_4$@$CoMoO_4$ electrode (2.452 F/cm^2) and $NiCo_2O_4$ electrode (0.456 F/cm^2). The total capacitance retention

of the $NiCo_2O_4$@$CoMoO_4$ and $NiCo_2O_4$@$NiMoO_4$ electrodes after 2000 cycles is ~95.5 and ~83.1 %, respectively. Based on these electrochemical properties, the $NiCo_2O_4$@$NiMoO_4$ composite electrode material may be more appropriate for practical applications.

Competing Interests
The authors declare that they have no competing interests.

Authors' Contributions
JH designed and performed the experiments. JH, GS, and FQ prepared the samples and analyzed the data. JH, GS, FQ, and LW participated in interpreting and analyzing the data. All authors read and approved the final manuscript.

Acknowledgements
We gratefully thank the Institute of Functional Nano & Soft Materials (FUNSOM) for supporting our work.

Author details
[1]No. 2 High School of East China Normal University, Shanghai 201203, China. [2]Institute of Functional Nano & Soft Materials (FUNSOM), Collaborative Innovation Center of Suzhou Nano Science and Technology, Soochow University, Suzhou, Jiangsu 215123, China. [3]College of Chemistry and Chemical Engineering, Shanghai University of Engineering Science, Shanghai 201620, China.

Received: 27 March 2016 Accepted: 9 May 2016
Published online: 18 May 2016

References
1. Simon P, Gogotsi Y (2008) Materials for electrochemical capacitors. Nat Mater 7:845
2. Wang GP, Zhang L, Zhang JJ (2012) A review of electrode materials for electrochemical supercapacitors. Chem Soc Rev 41:797
3. Liu C, Li F, Ma LP, Cheng HM (2010) Advanced materials for energy storage. Adv Mater 22:E28
4. Lu XH, Yu MH, Zhai T, Wang GM, Xie SL, Liu TY et al (2013) High energy density asymmetric quasi-solid-state supercapacitor based on porous vanadium nitride nanowire anode. Nano Lett 13:2628
5. Shen LF, Wang J, Xu GY, Li HS, Dou H, Zhang XG (2015) $NiCo_2S_4$ nanosheets grown on nitrogen-doped carbon foams as an advanced electrode for supercapacitors. Adv Energy Mater 5:1400977
6. Liu XY, Shi SJ, Xiong QQ, Li L, Zhang YJ, Tang H et al (2013) Hierarchical $NiCo_2O_4$@$NiCo_2O_4$ core/shell nanoflake arrays as high-performance supercapacitor materials. ACS Appl Mater Inter 5:8790
7. Bao FX, Zhang ZQ, Guo W, Liu XY (2015) Facile synthesis of three dimensional $NiCo_2O_4$@MnO_2 core-shell nanosheet arrays and its supercapacitive performance. Electrochim Acta 157:31
8. Li YH, Zhang YF, Li YJ, Wang ZY, Fu HY, Zhang XN et al (2014) Unveiling the dynamic capacitive storage mechanism of Co_3O_4@$NiCo_2O_4$ hybrid nanoelectrodes for supercapacitor applications Electrochim Acta 145:177
9. Liu XY, Zhang YQ, Xia XH, Shi SJ, Lu Y, Wang XL et al (2013) Self-assembled porous $NiCo_2O_4$ hetero-structure array for electrochemical capacitor. J Power Sources 239:157
10. Zhao JW, Chen JL, Xu SM, Shao MF, Zhang Q, Wei F et al (2014) Hierarchical NiMn layered double hydroxide/carbon nanotubes architecture with superb energy density for flexible supercapacitors. Adv Funct Mater 24:2938
11. Yan J, Fan ZJ, Sun W, Ning GQ, Wei T, Zhang Q et al (2012) Advanced asymmetric supercapacitors based on $Ni(OH)_2$/graphene and porous graphene electrodes with high energy density. Adv Funct Mater 22:2632
12. Lin TQ, Chen IW, Liu FX, Yang CY, Bi H, Xu FF et al (2015) Nitrogen-doped mesoporous carbon of extraordinary capacitance for electrochemical energy storage. Science 350:1509
13. Yang PH, Ding Y, Lin ZY, Chen ZW, Li YZ, Qiang PF et al (2014) Low-cost high-performance solid-state asymmetric supercapacitors based on MnO_2 nanowires and Fe_2O_3 nanotubes. Nano Lett 14:731
14. Zhang ZY, Chi K, Xiao F, Wang S (2015) Advanced solid-state asymmetric supercapacitors based on 3D graphene/MnO_2 and graphene/polypyrrole hybrid architectures. J Mater Chem A 3:12828
15. Wang X, Yan CY, Sumboja A, Lee PS (2014) High performance porous nickel cobalt oxide nanowires for asymmetric supercapacitor. Nano Energy 3:119
16. Xia XH, Chao DL, Fan ZX, Guan C, Cao XH, Zhang H et al (2014) A new type of porous graphite foams and their integrated composites with oxide/polymer core/shell nanowires for supercapacitors: structural design, fabrication, and full supercapacitor demonstrations. Nano Lett 14:1651
17. Xu KB, Huang XJ, Liu Q, Zou RJ, Li WY, Liu XJ et al (2014) Understanding the effect of polypyrrole and poly(3,4-ethylenedioxythiophene) on enhancing the supercapacitor performance of $NiCo_2O_4$ electrodes. J Mater Chem A 2:16731
18. Yuan CZ, Li JY, Hou LR, Zhang XG, Shen LF, Lou XW (2012) Ultrathin mesoporous $NiCo_2O_4$ nanosheets supported on Ni foam as advanced electrodes for supercapacitors. Adv Funct Mater 22:4592
19. Jiang H, Ma J, Li CZ (2012) Hierarchical porous $NiCo_2O_4$ nanowires for high-rate supercapacitors. Chem Commun 48:4465
20. Huang L, Chen DC, Ding Y, Feng S, Wang ZL, Liu ML (2013) Nickel-cobalt hydroxide nanosheets coated on $NiCo_2O_4$ nanowires grown on carbon fiber paper for high-performance pseudocapacitors. Nano Lett 13:3135
21. Chuo HX, Gao H, Yang Q, Zhang N, Bu WB, Zhang XT (2014) Rationally designed hierarchical $ZnCo_2O_4$/$Ni(OH)_2$ nanostructures for high-performance pseudocapacitor electrodes. J Mater Chem A 2:20462
22. Liu B, Zhang J, Wang XF, Chen G, Chen D, Zhou CW et al (2012) Hierarchical three-dimensional $ZnCo_2O_4$ nanowire arrays/carbon cloth anodes for a novel class of high-performance flexible lithium-ion batteries. Nano Lett 12:3005
23. Guo D, Luo YZ, Yu XZ, Li QH, Wang TH (2014) High performance $NiMoO_4$ nanowires supported on carbon cloth as advanced electrodes for symmetric supercapacitors. Nano Energy 8:174
24. Yang F, Zhao YL, Xu X, Xu L, Mai LQ, Luo YZ (2011) Hierarchical $MnMoO_4$/$CoMoO_4$ heterostructured nanowires with enhanced supercapacitor performance. Nat Commun 2:381
25. Yu XZ, Lu BG, Xu Z (2014) Super long-life supercapacitors based on the construction of nanohoneycomb-like strongly coupled $CoMoO_4$-3D graphene hybrid electrodes. Adv Mater 26:1044
26. Yuan CZ, Wu HB, Xie Y, Lou XW (2014) Mixed transition-metal oxides: design, synthesis, and energy-related applications. Angew Chem Int Ed 53:1488
27. Zhou C, Zhang YW, Li YY, Liu JP (2013) Construction of high-capacitance 3D CoO@polypyrrole nanowire array electrode for aqueous asymmetric supercapacitor. Nano Lett 13:2078
28. Xiao JW, Wan L, Yang SH, Xiao F, Wang S (2014) Design hierarchical electrodes with highly conductive $NiCo_2S_4$ nanotube arrays grown on carbon fiber paper for high-performance pseudocapacitors. Nano Lett 14:831
29. Yu GH, Xie X, Pan LJ, Bao ZN, Cui Y (2013) Hybrid nanostructured materials for high-performance electrochemical capacitors. Nano Energy 2:213
30. Liu JP, Jiang J, Cheng CW, Li HX, Zhang JX, Gong H et al (2011) Co_3O_4 nanowire@MnO_2 ultrathin nanosheet core/shell arrays: a new class of high-performance pseudocapacitive materials. Adv Mater 23:2076
31. Xu J, Wang QF, Wang XW, Xiang QY, Liang B, Chen D et al (2013) Flexible asymmetric supercapacitors based upon Co_9S_8 nanorod//Co_3O_4@RuO_2 nanosheet arrays on carbon cloth. ACS Nano 7:5453
32. Cheng D, Yang YF, Xie JL, Fang CJ, Zhang GQ, Xiong J (2015) Hierarchical $NiCo_2O_4$@$NiMoO_4$ core-shell hybrid nanowire/nanosheet arrays for high-performance pseudocapacitors. J Mater Chem A 3:14348
33. Yan T, Li RY, Zhou L, Ma CY, Li ZJ (2015) Three-dimensional electrode of Ni/Co layered double hydroxides@$NiCo_2S_4$@graphene@Ni foam for supercapacitors with outstanding electrochemical performance. Electrochimica Acta 176:1153
34. Zou RJ, Yuen MF, Yu L, Hu JQ, Lee CS, Zhang WJ (2016) Electrochemical energy storage application and degradation analysis of carbon-coated hierarchical $NiCo_2S_4$ core-shell nanowire arrays grown directly on graphene/nickel foam. Sci Rep 6:20624
35. Zou RJ, Zhang ZY, Yuen MF, Sun ML, Hu JQ, Lee CS, Zhang WJ (2015) Three-dimensional networked $NiCo_2S_4$ nanosheet arrays/carbon cloth anodes for high-performance lithium-ion batteries. NPG Asia Materials 7:e195
36. Zou RJ, Zhang ZY, Yuen MF, Hu JQ, Lee CS, Zhang WJ (2015) Dendritic heterojunction nanowire arrays for high-performance supercapacitors. Sci Rep 5:7862